Available online at www.sciencedirect.com

ScienceDirect

Journal of the European Ceramic Society 35 (2015) 703–709

www.elsevier.com/locate/jeurceramsoc

Inorganic foams made from alkali-activated fly ash: Mechanical, chemical and physical properties

P. Hlaváček [a,*], V. Šmilauer [a,*], F. Škvára [b], L. Kopecký [a], R. Šulc [a]

[a] Czech Technical University in Prague, Faculty of Civil Engineering, Thákurova 7, 166 29 Prague 6, Czech Republic

[b] Institute of Chemical Technology in Prague, Faculty of Chemical Engineering, Department of Glass and Ceramics, Technická 5, 166 28 Prague 6, Czech Republic

Received 28 June 2014; received in revised form 7 August 2014; accepted 12 August 2014

Available online 18 September 2014

Abstract

Alkali-activation of fly ash together with an aluminum powder blowing agent led to the synthesis of inorganic fly ash-based foam (FAF). The FAF is characterized by means of its compressive and flexural strength, thermal conductivity and capacity, exposure to high temperatures, performance in chemically aggressive environments, and 2D morphology. In comparison to traditional autoclaved aerated C-S-H-based materials, FAF retains exceptionally good fire resistance and high chemical durability, exhibits a rather closed-pore network, and requires temperatures below 80 °C for curing without the need for autoclaving. Experiments and micromechanical simulations prove that reasonable bulk densities lie in the range of 400–800 kg/m^3.

Keywords: Alkali-activation; Fly ash; Foam; Chemical durability; Thermal resistance

1. Introduction

Autoclaved aerated concrete (AAC) presents the most commonly used inorganic foam. AAC is a lightweight inorganic construction material exhibiting excellent combination of thermal and mechanical properties. The AAC is usually produced from a fine-grained cement mortar with the help of aluminum powder. The reaction between aluminum powder and alkalies from the cement mortar liberates hydrogen, thus increasing the total volume of the mixture. Successive autoclave treatment improves the compressive strength and reduces drying shrinkage.[1,2]

A cement-based AAC is a well-known material in Europe since 1920s. A Swedish architect Johann Erikksson patented the AAC in 1923. The first AAC manufacturer in the world was established in Sweden in 1929, and the use of a fly ash (FA) as a filler was first mentioned in Lindman's patent in 1931.[3]

Despite the long AAC history, only few authors mentioned aerated alkali-activated materials. In 1987, Costopoulos patented a fly ash-based aerated concrete.[4] He used fly ash class C or class F blended with ordinary Portland cement that was aerated either by (i) hydrogen peroxide releasing oxygen, (ii) a sodium carbonate releasing carbon dioxide, or (iii) acetic acid in a water solution. Prud'homme et al.,[5,6] on the other hand synthesized a geopolymer-based foam from dehydroxylated kaolinite activated by a solution of potassium hydroxide and potassium silicate, where silica fume served as a blowing agent. Delair et al.[7] examined the durability of a kaolinite-based geopolymeric foam in aqueous media. Bell and Kriven[8] prepared foams from metakaolin-based geopolymer, and Cilla et al.[9,10] created an open cell geopolymer foam. A review of geopolymer foam concrete can be found in Zhang et al.[11]

The world annual production of fly ashes is estimated to be around 600 million tons.[12] It is estimated that only 20–30% of FA is utilized, while the majority is dumped on landfills/lagoons, leading to an ecological burden. Several researchers have proved a successful utilization of fly ash by means of alkali-activation.[13–16] The alkali-activation generally presents a reaction between a strong alkaline liquid (e.g. a solution of sodium hydroxide and sodium metasilicate) and a solid

* Corresponding authors. Tel.: +420 22435 4482/4483.

E-mail addresses: petr.hlavacek@fsv.cvut.cz (P. Hlaváček), vit.smilauer@fsv.cvut.cz (V. Šmilauer), frantisek.skvara@vscht.cz (F. Škvára), kopecky@fsv.cvut.cz (L. Kopecký), rostislav.sulc@fsv.cvut.cz (R. Šulc).

http://dx.doi.org/10.1016/j.jeurceramsoc.2014.08.024

0955-2219/

Table 1
Chemical composition of fly ash (wt%).

	SiO_2	Al_2O_3	Fe_2O_3	CaO	K_2O	TiO_2
Fly ash	51.9	32.8	6.3	2.7	2.12	1.89

aluminosilicate material (e.g. fly ash, metakaolin or blast furnace slag). Depending on the authors, the reaction product is called soil-cement,[17] geopolymer,[18] inorganic polymer,[19] or alkali-activated material.[13,20–22] The stability of alkali-activated fly ashes has been proved by Wallah and Rangan by long term tests.[15] Further details on alkali-activated materials can be found elsewhere.[23–25]

In this paper, we design, synthesize, and optimize an alkali-activated fly ash foam (FAF) at temperatures below 80 °C. The FAF is a Portland cement-free, non-autoclaved, foam, composed of alkali-activated fly ash and aluminum powder. Hydrogen liberation during the activation process leads to a closed-pore network. A laboratory-scale production process is elaborated and mixture compositions undergo optimization for their pore distribution and bulk density.

The FAF compressive and flexural strength, thermal conductivity and capacity, and residual strength after exposure to high temperatures and aggressive environments are determined and compared with traditional AAC. Finite element simulations on 2D representations complement the understanding of the FAF elasticity. A long-term chemical durability test proves the stability and the closed pore nature of the produced FAF.

2. Materials and blowing process

The fly ash class F from the Opatovice brown coal power plant, Czech Republic (Blaine 210 m^2/kg) is used as the source material for alkali-activation, see Table 1 for the chemical composition. Fig. 1 shows the FA particle size distribution.

The aluminum metal powder (Al) from Albo Schlenk Inc., Bojkovice, Czech Republic, product type 76013 (average particle diameter by mass, $d_{50} \approx 35$ μm), is used as an air entraining agent.

Sodium hydroxide pellets dissolved in sodium metasilicate constitute the alkali activator. The composition of the alkali activator, i.e. the sodium hydroxide to metasilicate ratio, is taken from our previous research on alkali-activated fly ash.[16,22,26] The solid/liquid ratio and the amount of Al metal powder is optimized with respect to the FAF stability, porosity, and pore distribution. Fine tuning of the composition is done iteratively. The final compositions of the mixes are given in Table 2 and the corresponding pore structures are shown in Fig. 2.

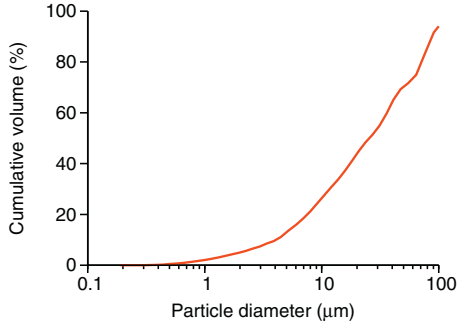

Fig. 1. The particle size distribution curve of fly ash used in experiments.

The reaction between the Al metal powder and the alkaline activator proceeds quickly, approximately as

$$2Al + 2NaOH + 2H_2O \rightarrow 2NaAlO_2 + 3H_2. \quad (1)$$

When 0.045 g of Al metal powder is mixed with 50 g of FA and an activator, there is approximately 15 s for stirring and casting a specimen. The hydrogen releases for about 1–2 min at ambient temperature. To reach a homogeneous pore distribution, the fly ash and Al metal powder are thoroughly mixed together in a dry state and the activator is added subsequently. Hand stirring takes place directly in a plastic form. Several attempts to mix the fly ash paste with the Al metal powder led to an improper pore distribution. The forms are kept under laboratory conditions at 22 °C for 2 h and subsequently put in the oven for 12 h at 80 °C. All specimens are prepared by cutting from larger bodies on a diamond saw.

Fig. 2 shows polished sections of the FAF with the mix compositions from Table 2. Since the proportions have four degrees of freedom, the composition of the activation solution is fixed and suitable ranges for liquid/solid and Al/solid ratios are determined experimentally.

The FAF nucleation and stability of the pore structure at the fresh state strongly depends on the viscosity of the initial mix. The viscosity can be easily tuned by the amount of added liquid activator, i.e. by the liquid/solid ratio. Our experiments indicate that liquid/solid ratios above 0.39 results in pastes with low viscosity, allowing rapid pore nucleation and, when all formed hydrogen gas leaves, a deflation. On the other hand, FAF produced with liquid/solid ratios under 0.37 results in high viscosity pastes that does not allow pore propagation; consequently, the corresponding specimens exhibit very low inflation. As it can be noticed in Fig. 2, the amount of Al metal powder has a less significant effect on the pore structure than the amount of liquid activator. The suitable amount of Al powder was found to be of approximately 0.1% of the fly ash mass.

For further testing, the composition FAF 5 is selected as the suitable representative of all mixes.

3. Methods

3.1. Mechanical properties

The uniaxial compressive test on 30 mm cubes provides the stress-strain diagram. The compressive strength is calculated from the peak load and the Young's modulus of elasticity is derived from the linear part of the stress-strain curve. Flexural strength is determined from a three point bending test on 40 mm × 40 mm × 160 mm prisms. Mechanical tests are performed on the TIRA test 2300 testing machine under a strain-controlled mode with deformation rate set at 0.5 mm/min.

Table 2
FAF compositions (the listed masses fill approximately the volume of 100 ml).

Mixture	FA (g)	Liquid/solid wt. (−)	NaOH (g)	Na metasilicate (g)	Al (g)	Bulk density (kg/m^3)
FAF 1	50	0.37	2.8	15.7	0.030	751
FAF 2	50	0.38	2.9	16.1	0.030	778
FAF 3	50	0.39	3.0	16.5	0.030	772
FAF 4	50	0.37	2.8	15.7	0.045	700
FAF 5	50	0.38	2.9	16.1	0.045	671
FAF 6	50	0.39	3.0	16.5	0.045	626
FAF 7	50	0.37	2.8	15.7	0.060	574
FAF 8	50	0.38	2.9	16.1	0.060	521
FAF 9	50	0.39	3.0	16.5	0.060	422

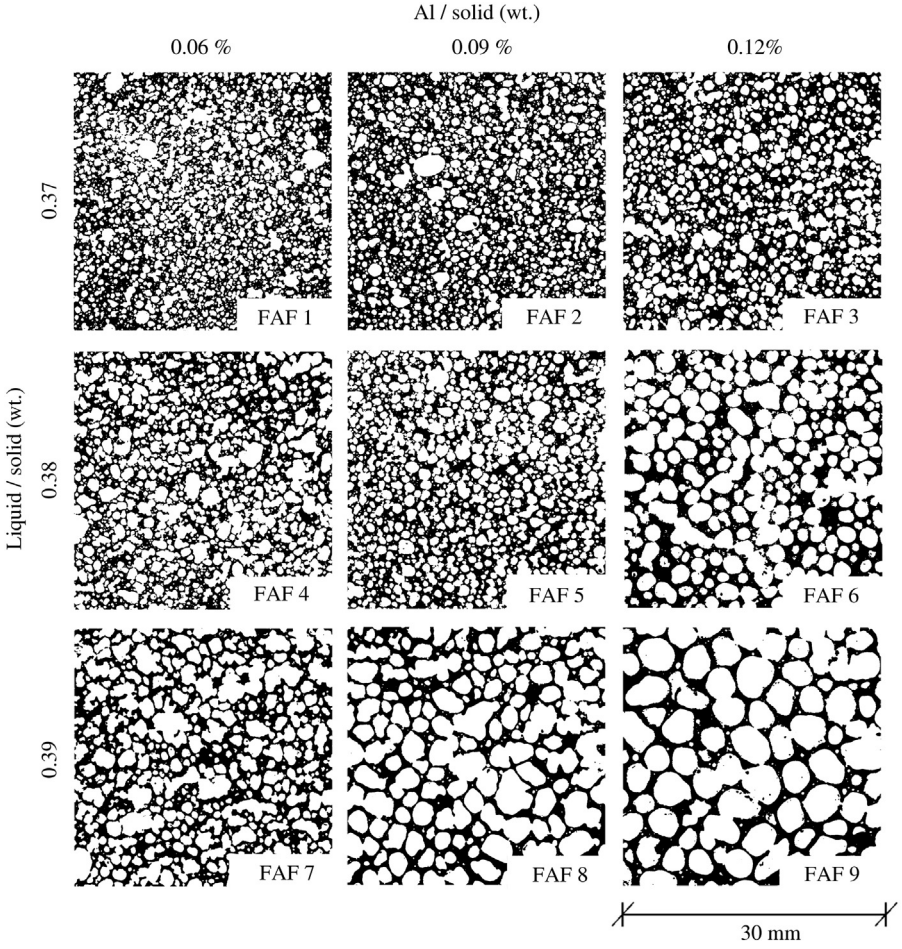

Fig. 2. The liquid/solid and Al/solid effect on the FAF pore distribution (pores are filled with an acrylic sealant).

3.2. Thermal conductivity and capacity

The thermal conductivity and volumetric heat capacity is measured on cylindrical specimens 15 mm thick and 70 mm in diameter under ambient conditions at 25 °C on Applied Precision, IZOMET 2104.

3.3. Chemical durability

The resistance to aggressive environments is quantified by a loss of compressive strength, reduction of elasticity, and a weight loss. The 30 mm FAF cubes are immersed in solutions of Na_2SO_4, $MgSO_4$, NaCl, H_2SO_4, and HCl. The concentrations of sulphates are taken from the European standard for concrete.[27] Due to the lack of appropriate standards for the performance of cements in acidic media, the pH of acids is taken from Allahverdi and Škvára,[28,29] see Table 3 for the concentrations. The FAF

Table 3
Details of chemical durability experiments.

Solution	Na_2SO_4	$MgSO_4$	NaCl	H_2SO_4	HCl
Concentration	44 g/l	5 g/l	164 g/l	pH 2	pH 2

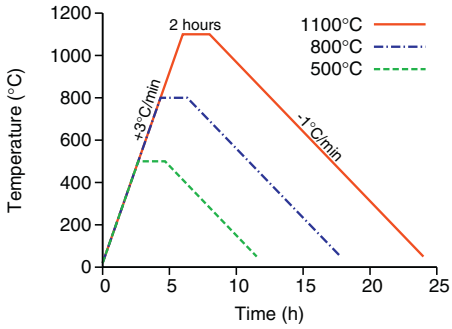

Fig. 3. Temperature profile during the fire resistance test.

cubes remain in the solutions for 90, 180 and 360 days, respectively. The solutions are replaced every 14 days to ensure a stable pH. The samples are removed and air-dried at 22 °C two days prior to compressive tests.

3.4. Fire resistance

The fire resistance test comprise temperature profiles according to Fig. 3. Prolonged exposures to 500 °C, 800 °C, and 1100 °C act on 30 mm FAF cubes. The volume changes, mass losses and stress-strain diagrams are recorded on cooled specimens.

4. Results and discussion

4.1. Mechanical and physical properties

Table 4 summarizes the measured bulk density ρ^b, the compressive strength f_{cm}, the flexural strength f_{tm}, the thermal conductivity λ and the thermal capacity c_p on FAF 5. The values always represent an average of at least four measurements. In addition, Table 4 mentions a traditional AAC with a similar bulk density as FAF 5.[30,31]

4.2. Chemical durability

Resistance to chemically aggressive environments is determined by a long-term exposure at ambient temperature. Table 5 shows the evolution of the compressive strength, Young's modulus and relative mass after 90, 180 and 360 days of exposure. The degree of pore saturation did not exceeded the value of 0.6 in any case, proving that the pores are of a closed nature.

The results from Table 5 show that the most severe degradation of FAF occurs in HCl and H_2SO_4 solutions. FAF deteriorates

Table 4
Data on FAF and traditional AAC.[30,31]

		FAF 5	AAC 600	AAC 675
Bulk density	ρ^b (kg/m^3)	671	600	675
Compressive strength	f_{cm} (MPa)	6.0	4.5	6.3
Flexural strength	f_{tm} (MPa)	1.0	0.85	1.0
Thermal conductivity	λ (W/m/K)	0.145	0.160	0.180
Thermal capacity	c_p (J/kg/K)	1089	–	–

Table 5
Compressive strength (f_{cm}), Young's modulus (E), and relative mass (m_r) of FAF 5 after chemical durability test.

	f_{cm} (MPa)			E (MPa)			m_r (–)		
	90	180	360	90	180	360	90	180	360
Na_2SO_4	5.30	4.72	5.13	773	731	602	0.97	0.94	0.96
$MgSO_4$	3.10	3.44	4.43	569	556	662	0.98	0.95	0.98
NaCl	3.27	3.77	2.68	511	526	409	1.00	0.99	1.00
H_2SO_4	2.30	1.60	1.21	218	203	28	0.87	0.79	0.75
HCl	1.74	1.34	1.21	181	145	37	0.86	0.79	0.76

by two mechanisms simultaneously. The first corresponds to Al depletion from N-A-S-H gel; specifically, the leaching leads to the ejection of Al from the aluminosilicate framework, leaving a relatively strong Si–O–Si skeleton.[28] Whereas the second mechanism corresponds to the dissolution of N-A-S-H gel in a low pH environment. According to our previous research on alkali-activated materials that were exposed to sulphate solutions, no new crystalline phases appear in XRD.[32] It is worthy to note that C-S-H gel would disintegrate almost completely under such an acid environment.[33]

4.3. Fire resistance

Fig. 4 shows the change of volume, mass, and color of FAF 5 after the fire-resistance test. Almost all chemically and physically bound water is removed already at 800 °C. The highest shrinkage increment appears between 800 °C and 1100 °C, which is related to gel sintering. The sintering leads to embodying Na directly in glass, implying a loss of efflorescence.[26]

Table 6 displays the evolution of compressive strength and Young's modulus. The increase of compressive strength and Young's modulus for samples loaded by 1100 °C can be explained by N-A-S-H gel transformation into glass.

4.4. Homogenization of Young's modulus

Effective Young's modulus provides useful information on the microstructure, especially the interconnectedness of phases and their intrinsic elastic properties. A 2D scan of FAF 5 (see

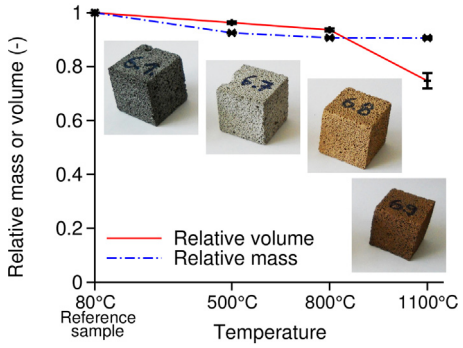

Fig. 4. Relative changes of mass and volume of FAF 5 with standard deviations.

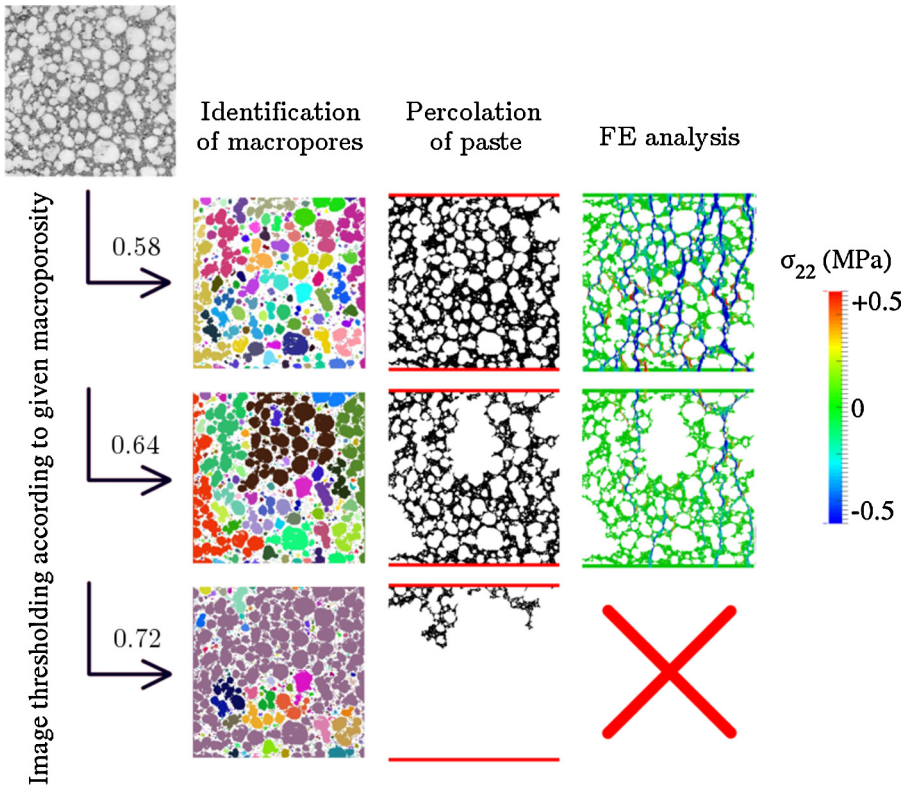

Fig. 5. Image processing of FAF 5: thresholding, identification, percolation, stress σ_{22} under $\langle\varepsilon_{22}\rangle = 0.0001$.

Fig. 5) gives a starting microstructure for a numerical analysis aiming at simulating the effective Young's modulus.

The porosity of FAF can be divided into two groups. The first one represents small micropores (<100 μm), which reside in the activated fly ash paste. The second group are macropores (>100 μm) creating the FAF pore structure. The macroporosity of the specimens ϕ^{macro} is calculated from a known bulk density of the paste $\rho^{\text{b}}_{\text{paste}} = 1752$ kg/m^3 [22] and the measured FAF bulk density ρ^{b}_{foam}

$$\phi^{\text{macro}} = 1 - \frac{\rho^{\text{b}}_{\text{foam}}}{\rho^{\text{b}}_{\text{paste}}}. \quad (2)$$

The role of macroporosity on elasticity is explored on a 2D scan of FAF 5. The image is converted to 256 grayscales and 13 meshes generated with macroporosities in the range of 0.50–0.74 in 0.02 increments. Fig. 5 shows three selected macroporosity values.

Table 6
Compressive strength (f_{cm}) and Young's modulus (E) of FAF after fire-resistance test, standard deviations in parentheses.

Temperature	f_{cm} (MPa)	E (MPa)
Reference 80 °C	5.99 (1.61)	833.8 (140.0)
500 °C	6.74 (1.82)	776.9 (116.2)
800 °C	5.13 (1.04)	734.1 (110.9)
1100 °C	13.25 (2.96)	1349.5 (188.4)

A burning algorithm explores the paste connectedness within the images. All connected paths are identified and disconnected parts from the edges eliminated. As the macroporosity increases, several unconnected paste clusters emerge. The ratio of the pixels that remains after the burning algorithm to the original amount is called solid percolation. Fig. 6 shows the extent. The solid percolation threshold represents the macroporosity where no path between the top and the bottom exists. In our particular case, this corresponds to a macroporosity of 0.72, which equals the FAF bulk density of 490 kg/m^3. However, the solid percolation threshold in 3D would be higher due to out-of-plane solid paths.[34] This result is in agreement with the lowest bulk density of 400 kg/m^3 measured in our experiments.

The burnt images, see percolation of paste in Fig. 5, serve for creating a mesh where each black pixel corresponds to one

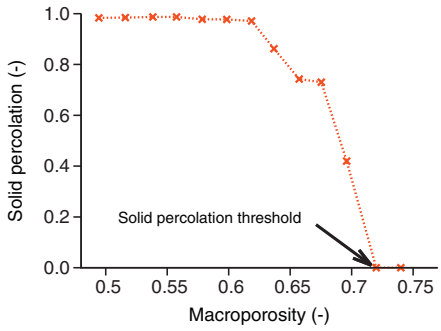

Fig. 6. Solid percolation of FAF for different macroporosities.

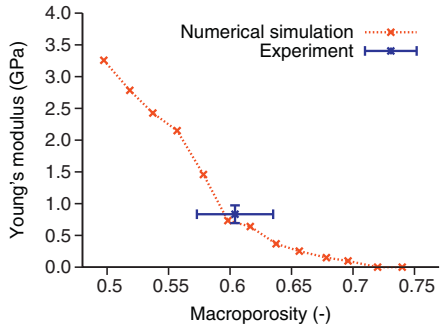

Fig. 7. Young's modulus for various macroporosities.

linear quadrilateral finite element. The regular mesh has 500×500 elements with an element size of 40 μm. Since the porosity is not meshed, the resulting mesh contains between 70,000 and 130,000 finite elements. The horizontal edges are loaded by kinematic uniform boundary conditions in the form of a prescribed displacement, while the vertical edges are kept free. The intrinsic Young's modulus of alkali-activated paste is of 35.35 GPa and the Poisson's ratio is set at 0.2; these values correspond to the degree of fly-ash reaction of 0.59 from our previous research.[22] Fig. 5 shows the sequence up to the final FE analysis.

The averaged vertical stress and strain provide the effective Young's modulus

$$E_{eff} = \frac{\langle \sigma_{22} \rangle}{\langle \varepsilon_{22} \rangle}, \tag{3}$$

which is shown in Fig. 7 for different macroporosities. The experimental modulus agrees well with the simulation results.

5. Conclusion

Fly ash, alkali activator, and aluminum powder led to the design, synthesis and optimization of fly ash foam (FAF). Variations in input materials proved feasible bulk densities in the range of 400–800 kg/m^3. The initial mix viscosity was found crucial in the preparation process. Characteristic samples with bulk density of 671 kg/m^3 exhibit similar properties to commercially produced autoclaved aerated concrete in terms of mechanical and thermal properties. FAF exhibit major benefits over traditional aerated materials:

- high fire resistance up to 1100 °C accompanied by high shrinkage and material sintering;
- long-term chemical durability in a liquid aggressive environment of Na_2SO_4, $MgSO_4$, NaCl, H_2SO_4, and HCl. The durability stems mainly from a closed-pore network and absence of leachable Ca in the FAF;
- fly ash utilization and the absence of autoclaving.

Acknowledgements

The authors are grateful to M. Vokáč for conducting mechanical tests and P. Semerák for measurements of thermal properties. Financial support from the Czech Science Foundation under the project GAP104/12/0102 is gratefully acknowledged for experimental part while the project GA13-22230S is appreciated for numerical simulations.

References

1. Narayanan N, Ramamurthy K. Structure and properties of aerated concrete: a review. *Cem Concr Compos* 2000;**22**:321–9.
2. Jerman M, Keppert M, Výborný J, Černý R. Hygric, thermal and durability properties of autoclaved aerated concrete. *Constr Build Mater* 2013;**41**:352–9.
3. Pytlik RC, Saxena J. Autoclaved cellular concrete: the building material for the 21st century. In: Wittmann FH, editor. *Advances in autoclaved aerated concrete*. Rotterdam/Brookfield: A.A. Balkema; 1992. p. 1–18.
4. Costopoulos NG, Newhouse HK. Building material manufacturing from fly ash. US Patent 4,659,385; 1987.
5. Prud'homme E, Michaud P, Joussein E, Peyratout C, Smith A, Arrii-Clacens S, et al. Silica fume as porogent agent in geo-materials at low temperature. *J Eur Ceram Soc* 2010;**30**:1641–8.
6. Prud'homme E, Michaud P, Joussein E, Peyratout C, Smith A, Rossignol S. In situ inorganic foams prepared from various clays at low temperature. *Appl Clay Sci* 2011;**51**:15–22.
7. Delair S, Prud'homme E, Peyratout C, Smith A, Michaud P, Eloy L, et al. Durability of inorganic foam in solution: the role of alkali elements in the geopolymer network. *Corros Sci* 2012;**59**:213–21.
8. Bell JL, Kriven WM. Preparation of ceramic foams from metakaolin-based geopolymer gels. In: Lin HT, Koumoto K, Kriven WM, Garcia E, Reimanis IE, Norton DP, editors. *Developments in strategic materials, Ceram Eng Sci Proc*. New Jersey: John Wiley & Sons Inc.; 2009. p. 97–112, 29.
9. Cilla MS, Colombo P, Morelli MR. Geopolymer foams by gelcasting. *Ceram Int* 2014;**40**:5723–30.
10. Cilla MS, Morelli MR, Colombo P. Open cell geopolymer foams by a novel saponification/peroxide/gelcasting combined route. *J Eur Ceram Soc* 2014;**34**:3133–7.
11. Zhang Z, Provis JL, Reid A, Wang H. Geopolymer foam concrete: an emerging material for sustainable construction. *Constr Build Mater* 2014;**56**:113–27.
12. Ahmaruzzaman M. A review on the utilization of fly ash. *Prog Energ Combust* 2010;**36**:327–63.
13. Shi C, Krivenko PV, Roy D. *Alkali-activated cements and concretes*. 1st ed. Oxon: Taylor & Francis; 2006.
14. Fernandez-Jimenez A, Palomo A. Characterisation of fly ashes. Potential reactivity as alkaline cements. *Fuel* 2003;**82**:2259–65.
15. Wallah SE, Rangan BV. *Low-calcium fly ash-based geopolymer concrete: long term properties. Res. Report-GC2*. Perth, Australia: Curtin University of Technology; 2006.
16. Škvára F, Kopecký L, Šmilauer V, Bittnar Z. Material and structural characterization of alkali activated low-calcium brown coal fly ash. *J Hazard Mater* 2009;**168**:711–20.
17. Glukhovsky VD. *Soil silicates (Gruntosilikaty)*. Kiev: Budivelnik Publisher; 1959.
18. Davidovits J. Synthesis of new high-temperature geo-polymers for reinforced plastics/composites. In: *Proceedings of PACTEC'79*. Society of Plastic Engineers; 1979. p. 151–4.
19. Van Jaarsveld J, Van Deventer J, Lukey G. The effect of composition and temperature on the properties of fly ash-and kaolinite-based geopolymers. *Chem Eng J* 2002;**89**:63–73.
20. Palomo A, Grutzeck MW, Blanco MT. Alkali-activated fly ashes. A cement for the future. *Cem Concr Res* 1999;**29**:1323–9.
21. Fernández-Jiménez A, Palomo A. Composition and microstructure of alkali activated fly ash binder: effect of the activator. *Cem Concr Res* 2005;**35**:1984–92.
22. Šmilauer V, Hlaváček P, Škvára F, Šulc R, Kopecký L, Němeček J. Micromechanical multiscale model for alkali activation of fly ash and metakaolin. *J Mater Sci* 2011;**46**:6545–55.

23. Duxson P, Fernández-Jiménez A, Provis JL, Lukey GC, Palomo A, van Deventer JSJ. Geopolymer technology: the current state of the art. *J Mater Sci* 2007;**42**:2917–33.
24. Pacheco-Torgal F, Castro-Gomes J, Jalali S. Alkali-activated binders: a review. Part 1. Historical background, terminology, reaction mechanisms and hydration products. *Constr Build Mater* 2008;**22**:1305–14.
25. Provis JL, van Deventer JSJ. *Geopolymers: structures, processing, properties and industrial applications*. 1st ed. Oxford/Cambridge/New Delhi: Woodhead Publishing Ltd.; 2009.
26. Škvára F, Šmilauer V, Hlaváček P, Kopecký L, Cílová Z. A weak alkali bond in (N, K)–A–S–H gels: evidence from leaching and modeling. *Ceram-Silikaty* 2012;**56**:374–82.
27. EN 206-1:2000, Concrete – Part 1: specification, performance, production and conformity. European Committee for Standardization; 2000.
28. Allahverdi A, Škvára F. Acidic corrosion of hydrated cement based materials. *Ceram-Silikaty* 2000;**44**:152–60.
29. Allahverdi A, Škvára F. Sulfuric acid attack on hardened paste of geopolymer cements. Part 2. Corrosion mechanism at mild and relatively low concentrations. *Ceram-Silikaty* 2006;**50**:1–4.
30. Neville AM. *Properties of Concrete*. New Jersey: John Wiley & Sons Inc.; 1997.
31. Building Research Establishment Autoclaved aerated concrete. BRE Digest 1989; 342.
32. Jílek T. *Vliv agresivního prostředí na vlastnosti geopolymerních materiálů Thesis in Czech*. Prague: Institute of Chemical Technology; 2006.
33. Constantinides G, Ulm FJ. The effect of two types of C-S-H on the elasticity of cement-based materials: results from nanoindentation and micromechanical modeling. *Cem Concr Res* 2004;**34**:67–80.
34. Bentz DP, Garboczi EJ, Snyder KA. *A hard core/soft shell microstructural model for studying percolation and transport in three-dimensional composite media. Res. Report*. Gaithersburg, MD: NIST Building and Fire Research Laboratory; 1999.